PCCP

COMMUNICATION

View Article Online
View Journal | View Issue

Cite this: *Phys. Chem. Chem. Phys.*, 2016, **18**, 694

Received 20th October 2015,
Accepted 30th November 2015

DOI: 10.1039/c5cp06381g

www.rsc.org/pccp

Packing morphology of wavy nanofiber arrays†

Itai Y. Stein*[a] and Brian L. Wardle[b]

Existing theories for quantifying the morphology of nanofibers (NFs) in aligned arrays either neglect or assume a simple functional form for the curvature of the NFs, commonly known as the NF waviness. However, since such assumptions cannot adequately describe the waviness of real NFs, errors that can exceed 10% in the predicted inter-NF separation can result. Here we use a theoretical framework capable of simulating $>10^5$ NFs with stochastic three-dimensional morphologies to quantify NF waviness on an easily accessible measure of the morphology, the inter-NF spacing, for a range of NF volume fractions. The presented scaling of inter-NF spacing with waviness is then used to study the morphology evolution of aligned carbon nanotube (A-CNT) arrays during packing, showing that the effective two-dimensional coordination number of the A-CNTs increases much faster than previously reported during close packing, and that hexagonal close packing can successfully describe the packing morphology of the A-CNTs at volume fractions greater than 40 vol%.

One dimensional nanostructures, such as nanowires, nanofibers (NFs), and nanotubes have attracted much attention due to their exciting intrinsic mechanical,[1–6] thermal,[1–3,7–9] and electrical properties.[1–3,9–11] However, such theoretical properties are still elusive, and cannot currently be attained in scalable architectures, such as NF arrays, that are comprised of $>10^9$ NFs cm^{-2}.[1] One of the primary reasons that the exceptional intrinsic properties of NFs cannot be achieved in large structures is the morphology of real NFs, which have some degree of curvature that is commonly known as waviness.[12,13] But in most cases, the NF waviness is either assumed to be of a simple function form, *e.g.* sinusoidal or helical,[14–19] or neglected altogether.[20–26] This stems in part from the lack of an accessible theoretical framework that can be used to quantify the impact of waviness on the packing morphology of real NFs in three-dimensions. In this report, we use a simulation framework in conjunction with an existing continuous coordination number theoretical framework to evaluate the influence of NF waviness on the morphology of an exemplary NF system, carbon nanotube (CNT) arrays.

By assuming a sinusoidal functional form characterized by the ratio of the amplitude (a) and wavelength (λ) of the sine waves, known as the waviness ratio ($w = a/\lambda$), previous studies have shown that the waviness of CNTs is significant with $w \gtrapprox 0.2$ for as-synthesized vertically aligned CNT (A-CNT) arrays.[27–29] See Fig. 1a for a high resolution scanning electron micrograph of the cross-sectional morphology of as-grown A-CNTs demonstrating their significant waviness. Such non-idealities were previously shown to strongly impact the mechanical behavior of CNTs and their architectures,[13–18] where orders of magnitude reductions in stiffness of the CNTs can result from small degrees of local curvature.[13,30] However, although CNTs that comprise scalable arrays have waviness/tortuosity that is not negligible,[31–34] is directly tied to the parameters used in the synthesis process,[33,34] and strongly impacts their behavior,[33,34] existing theoretical models can only work with idealized collimated A-CNTs ($w = 0$).[35,36] These models mention that since a precise description of the CNT waviness was not available at the time, further work is required to appropriately account for waviness when modeling the evolution of the CNT packing morphology.[35] Here we study aligned arrays comprised of 10^5 simulated CNTs with realistic morphologies, and show how waviness impacts an easily accessible measure of the morphology, the average inter-CNT spacing, and the effective 2D coordination number that specifies their packing geometry. See Fig. 1b for an illustration of the idealized collimated A-CNTs studied in previous work, and the simulated wavy A-CNTs studied here.

To simulate wavy NFs, each NF was discretized into an array of nodes in three dimensions (xyz space). The position of the

[a] *Department of Mechanical Engineering, Massachusetts Institute of Technology, 77 Massachusetts Ave., Cambridge, MA 02139, USA. E-mail: iys@mit.edu*
[b] *Department of Aeronautics and Astronautics, Massachusetts Institute of Technology, 77 Massachusetts Ave., Cambridge, MA 02139, USA*

† Electronic supplementary information (ESI) available: Illustration of the constitutive triangles that comprise the two-dimensional coordination number (Fig. S1), power scaling equations and table of numerical values for waviness correction of square and hexagonal packing (eqn (S1) and (S2), Table S1), equations and plot of waviness scaling with carbon nanotube (CNT) volume fraction (eqn (S3) and Fig. S2), and tables of the simulation-evaluated waviness corrected CNT separation and coordination numbers (Tables S2 and S3). See DOI: 10.1039/c5cp06381g

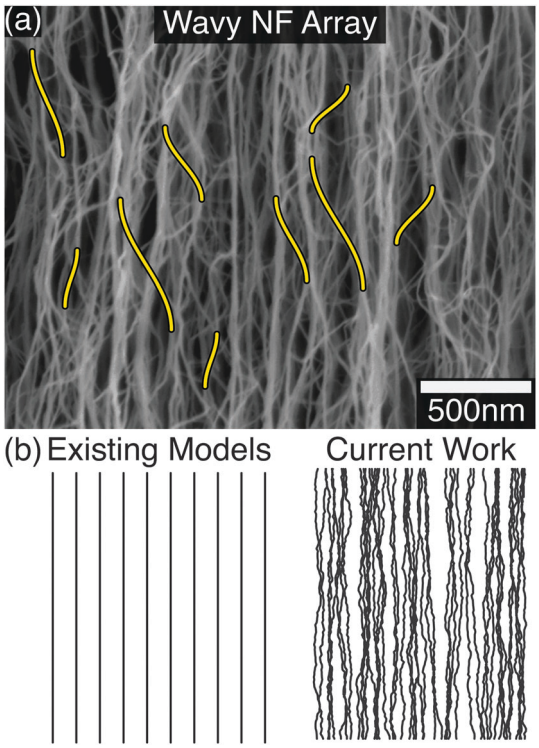

Fig. 1 Real wavy nanofibers (NFs) and theoretical frameworks. (a) Representative high resolution scanning electron microscopy image of wavy arrays of NFs, specifically carbon nanotubes. (b) Illustration of the NF morphology normally assumed in existing theoretical frameworks, which neglect the NF waviness, and the wavy NFs with realistic stochastic morphologies generated using the simulation framework presented here.

first node was determined using the constitutive triangles that are defined by the two-dimensional ($x-y$ plane) coordination number (N), which was discussed in detail previously.[35,36] See Fig. S1 in the ESI,† for illustration of the constitutive triangles that define each N. Since values of N that fall between square ($N = 4$) and hexagonal ($N = 6$) close packing may not propagate properly in the $x-y$ plane, NFs were initialized in layers, and each layer was arranged in a manner analogous to Bernal stacking (*i.e.* ABAB type stacking) to facilitate the formation of constitutive triangles with appropriate dimensions as defined by N and the volume fraction of the NFs (V_f).[35] See Fig. 2a for an illustration of the layer-like arrangement of the first nodes of the discretized NFs, and for exemplary initialized simulations comprised of 100 NFs ($\rightarrow n = 100$) for $N = 4$ and $N = 6$. To apply the appropriate waviness to all other nodes, the displacement of each node relative to the node that precedes it, defined as Δr, was evaluated using the amplitude (a) extracted from the waviness ratio (w), and the node displacement increment in the $\hat{z}$ direction was set at a magnitude of 0.05λ, where λ is the wavelength of the waviness ($\rightarrow \lambda = a/w$) that has a value equal to the maximum inter-NF spacing,[30,36] so that a unit cell comprised of 10 nodes (see Fig. 2b for illustration) will have a total $\hat{z}$ displacement, defined as Δz, of magnitude $\lambda/2$. Since the waviness of the NFs is inherently random, the displacement specified by the evaluated a was independently applied to the nodes of the NF in both x and y directions using Gaussian distributions.

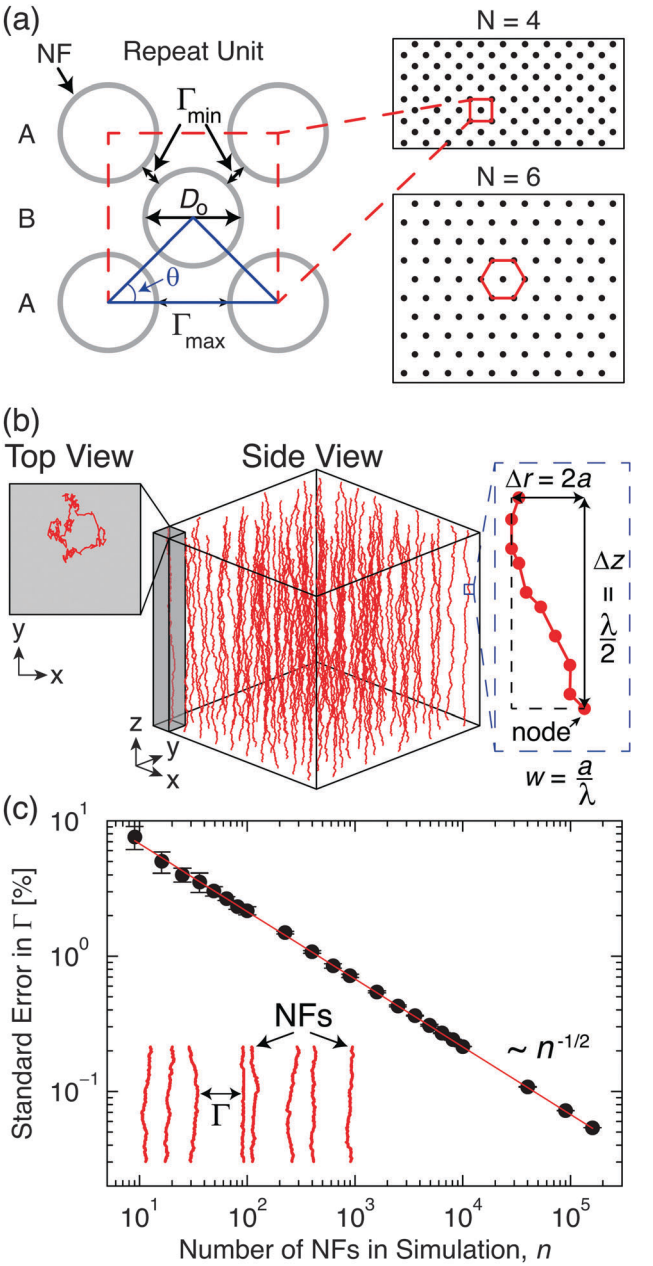

Fig. 2 Simulation details and standard error scaling. (a) Illustration of the simulation scheme, origin of the inter-nanofiber (NF) spacing (Γ) from the two-dimensional coordination number (N), and top view of an initialized simulation cell comprised of collimated 100 NFs for $N = 4$ (square packing) and $N = 6$ (hexagonal packing). (b) Initialized simulation comprised of 100 wavy NFs showing how the average node displacements in the $x-y$ plane and $\hat{z}$ direction are tied to the amplitude (a) and wavelength (λ) that originate from the waviness ratio ($w = a/\lambda$) and used to generate wavy NFs. (c) Scaling in standard error of the measured Γ values demonstrating the importance of number of NFs in the simulation (n), and replicating the familiar $1/\sqrt{n}$ standard error scaling for Gaussian statistics.

Using Gaussian distributions to apply the node displacements has two distinct advantages: (1) the mean and standard deviations (normally $\gtrapprox 50\%$ of the mean values)[27,28,30] of w can be used to directly specify the waviness, which may not be true for other distributions; (2) the node displacements are no longer

uniform nor deterministic, *e.g.* as in cases where sinusoidal or helical functional forms were assumed,[14–18] leading to more realistic morphologies. Also, while the current method does not explicitly account for NF–NF interactions, *e.g.* van der Waals (vdW) interactions used in recent modeling efforts,[37–39] in the three-dimensional morphology evolution, the stochastic nature of the NF array morphology implicitly accounts for the attractive and repulsive forces that would be experienced by the NFs, while avoiding the assumption of a simplistic electrostatic potential that may not be representative for NFs with native defects and other adsorbed species.[36] The main difference between the current method, and modeling efforts that include electrostatic interactions, is that NF arrays simulated here might form fewer bundles/aggregates, but such an effect will be very small when averaged over a sample size of $>10^5$ NFs. See Fig. 2b for a top-view snapshot of a single wavy NF along the $\hat{z}$ direction demonstrating the random-walk like nodal displacement, and for a side view snapshot of a simulation comprised of $n = 100$ wavy NFs. To ensure that the waviness generated using the scheme used here is consistent with the amount of waviness that would result if a simple sinusoidal functional form was used instead, the separation of the nodes in the $\hat{z}$ direction was adjusted so that the ratios of the true length of the NF (L) to the measured height of the NF in the $\hat{z}$ direction (H) for both schemes were matched. The L/H ratio is a common way to evaluate the tortuosity of the NFs, and since the tortuosity does not depend on the functional form (*i.e.* a, and λ) of the waviness, the L/H ratio is a more flexible measure by which the waviness of NFs can be quantified and compared between systems.

To quantitatively evaluate the impact of waviness on the morphology of the aligned NF arrays, a measure that can be easily approximated experimentally was selected: the average inter-NF spacing (Γ). To approximate Γ for the simulated wavy NFs, the difference in position in the $x-y$ plane for each NF was calculated using the separation of the current NF, for example a NF in the center of a square unit cell located in layer B (see Fig. 2a for an illustration), with its neighboring NFs as follows: the inter-NF separation for NFs in the same layer, *i.e.* the two neighboring NFs in layer B for the exemplary NF, which yields the maximum inter-NF spacing; and the inter-NF separation for NFs in adjacent layers, *i.e.* the four neighboring NFs in the two C layers (above and below) for the exemplary NF yielding the minimum inter-NF spacing. Γ was approximated by simply taking the average of the minimum and maximum inter-NF spacings.[35] The NFs on the outer boundary were treated differently to account for the missing neighbor NFs, but have a very small contribution $\ll 0.1\%$ overall if sufficiently large simulation cells are used ($n \gtrapprox 1600$). The contribution of the NF waviness to Γ was included in the analysis as follows:

$$\Gamma(w) = \Omega(w)\Gamma(w = 0) \quad (1)$$

where Ω is the waviness correction with a value that is >1 for $w > 0$, and $\Gamma(w = 0)$ is evaluated using N and the NF V_f using the previously reported theoretical framework.[35] To approximate the accuracy of the current measurement, the standard error of Γ was evaluated as a function of n, and is plotted in Fig. 2c. As Fig. 2c demonstrates, the familiar standard error scaling of $\propto 1/\sqrt{n}$ is exhibited, and to ensure a standard error of $\lesssim 0.1\%$, a simulation size of $n > 10^5$ ($\rightarrow 320 \times 320 = 1.024 \times 10^5$ NFs) is used throughout this report. This simulation framework can be used to study NF arrays comprised of non-interacting NFs with V_f up to 40 vol% NFs, which means that the results of the morphology analysis will be physical for the entire range of experimentally accessible V_f for NF arrays prepared using mechanical densification.

Since square ($N = 4$) and hexagonal ($N = 6$) packing are the most commonly assumed coordinations,[35] but their sensitivity to NF waviness is not currently known, the average inter-NF spacing (Γ) was evaluated as a function of the waviness ratio (w) for $0 \leq w \leq 0.3$ which are representative of the typical range of the experimentally observed NF waviness.[30,40,41] Using Γ at $w = 0$ ($\rightarrow \Gamma(w = 0)$), *i.e.* morphology of idealized collimated NFs, the waviness correction for $N = 4$ ($\rightarrow \Omega_{\square}$) and $N = 6$ ($\rightarrow \Omega_{\hexagon}$) was evaluated *via* eqn (1). See Fig. 3 for plots demonstrating the scaling of $\Omega_{\square}$ and $\Omega_{\hexagon}$ with w. As Fig. 3a demonstrates, the scaling of $\Omega_{\square}$ with w can be described by power laws at three different regimes (see eqn (S1) and Table S1 in the ESI,† for details): (1) $0 \leq w < 0.05$, (2) $0.05 \leq w \leq 0.125$, and (3) $0.125 < w \leq 0.3$. These three modes are consistent with (1) initiation, where the NFs are just starting to fill the inter-NF

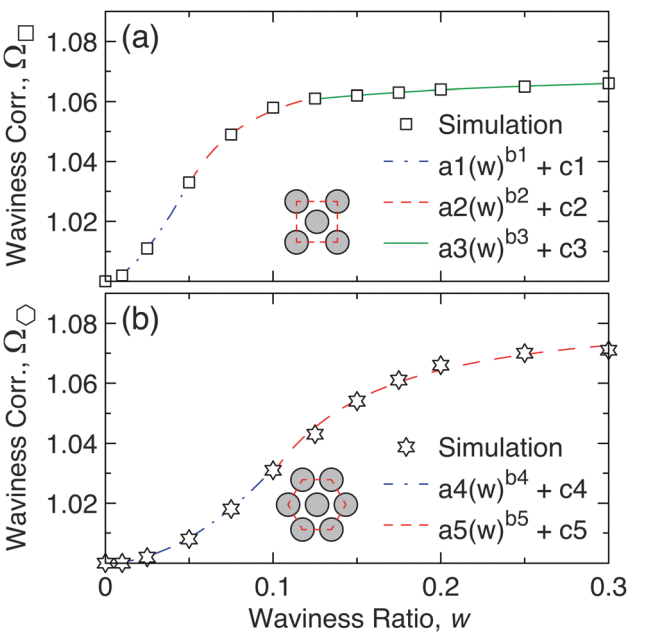

Fig. 3 Impact of waviness (w) on the packing morphology of NF arrays exhibiting square and hexagonal close packing. (a) Evolution of the waviness correction (see eqn (1)) for square packing ($\Omega_{\square}$) as a function of w showing that the scaling of $\Omega_{\square}$ can be represented by three power laws at $w < 0.05$, $0.05 \leq w \leq 0.125$, and $w > 0.125$, and that square packing is best suited for NF systems with $w \gtrapprox 0.15$ where $\Omega_{\square}$ increases very gradually. (b) Scaling of the waviness correction (see eqn (1)) for hexagonal packing ($\Omega_{\hexagon}$) with w showing that $\Omega_{\hexagon}$ can be described by two power laws at $w < 0.1$, and $w \geq 0.1$, and that hexagonal packing is best suited for NF systems with $w \gtrapprox 0.05$ where <1% error will be induced by neglecting the NF waviness.

region, (2) crowding, where the NFs are starting to feel their bounding box that is characteristic of the formation of significant NF bundles/junctions, and (3) saturation, where the NFs have already filled up most of the inter-NF space and are slowly adding more NF junctions/bundles. Fig. 3a also indicates that $\Omega_{\square}$ is nearly constant at $w \gtrapprox 0.15$, where $\Omega_{\square} \approx 1.07$, meaning that square close packing is best suited for approximating the morphology of NF arrays with significant waviness. As Fig. 3b illustrates, the evolution of $\Omega_{\hexagon}$ with w is characteristic of power laws at two different regimes (see eqn (S2) and Table S1 in the ESI,† for details): (1) $0 \leq w \leq 0.1$, (2) $0.1 < w \leq 0.3$. The first two modes are consistent with the initiation and crowding modes of $\Omega_{\square}$, but since the first two modes span larger regimes for $\Omega_{\hexagon}$, and the saturation mode is not yet seen in Fig. 3b, the saturation mode of $\Omega_{\hexagon}$ will occur later at $w > 0.3$. Also, since the first mode of $\Omega_{\hexagon}$ extends up to $w \approx 0.1$, Fig. 3b indicates that hexagonal close packing will be best for NFs with a small amount of waviness, where neglecting waviness will not incur a significant amount of error in the average packing morphology. Since $\Omega_{\square}$ and $\Omega_{\hexagon}$ are non-dimensional ratios of Γ that natively include the NF diameter contribution, the results presented in Fig. 3 are independent of the NF diameter. To properly account for waviness in real NF arrays, where N is not constant, the previously reported scaling of Γ in an exemplary system of A-CNTs (Γ_{cnt}) as a function of the CNT volume fraction ($V_{\mathrm{f,cnt}}$) is explored,[35] and the recently reported scaling of w for this system as a function of $V_{\mathrm{f,cnt}}$ is used to quantify the evolution of N as a function of CNT packing.[30]

Recent experimental work has demonstrated that, in an exemplary system of chemical vapor deposition (CVD) grown millimeter-long A-CNTs,[35,36] Γ_{cnt} is reduced from $\sim$80 nm to $\sim$10 nm as $V_{\mathrm{f,cnt}}$ is increased from $\sim$1 vol% CNTs to $\sim$20 vol% CNTs.[35] See Fig. 4a for the previously reported experimental values of Γ_{cnt}. To better understand and model how Γ_{cnt} and the waviness correction for CNTs (Ω_{cnt}) scales with $V_{\mathrm{f,cnt}}$, the previous work assumed that the CNTs are collimated (*i.e.* not wavy), and using a continuous two-dimensional coordination number (N) model, extracted the effective coordination number at each $V_{\mathrm{f,cnt}}$.[35] Using the theoretical data point of $N = 6$ at $V_{\mathrm{f,cnt}} = 83.4\%$ CNTs, the previous study showed that N scales linearly with $V_{\mathrm{f,cnt}}$ (see Fig. 4b).[35] Such a scaling relation assumes that very few CNT bundles form throughout the range of $V_{\mathrm{f,cnt}}$, which might be reasonable for $V_{\mathrm{f,cnt}} \gtrapprox 20\%$ CNTs (where experimental data was provided),[35] but is likely not true for $V_{\mathrm{f,cnt}} > 20\%$ where the formation of CNT bundles with $N = 6$ is more pronounced. The key limitation of the previous analysis was that the CNT waviness could not be integrated into the Γ_{cnt} description used to calculate N, which can lead to errors in the evaluated N, as shown in Fig. 3. Using the recently reported experimental scaling relation of the mean and standard deviation of w with $V_{\mathrm{f,cnt}}$ ($\rightarrow w(V_{\mathrm{f,cnt}}) = -0.04967(V_{\mathrm{f,cnt}})^{0.3646} + 0.2489 \pm -0.0852(V_{\mathrm{f,cnt}})^{0.2037} + 0.21$),[30] the scaling of Γ_{cnt} and Ω_{cnt} with $V_{\mathrm{f,cnt}}$ was simulated and can be found in Fig. 4a. As Fig. 4a demonstrates, the simulated scaling of Γ_{cnt} with $V_{\mathrm{f,cnt}}$ agrees very well with both the experimental and previous theoretical model results,[35] and Ω_{cnt} scales linearly with

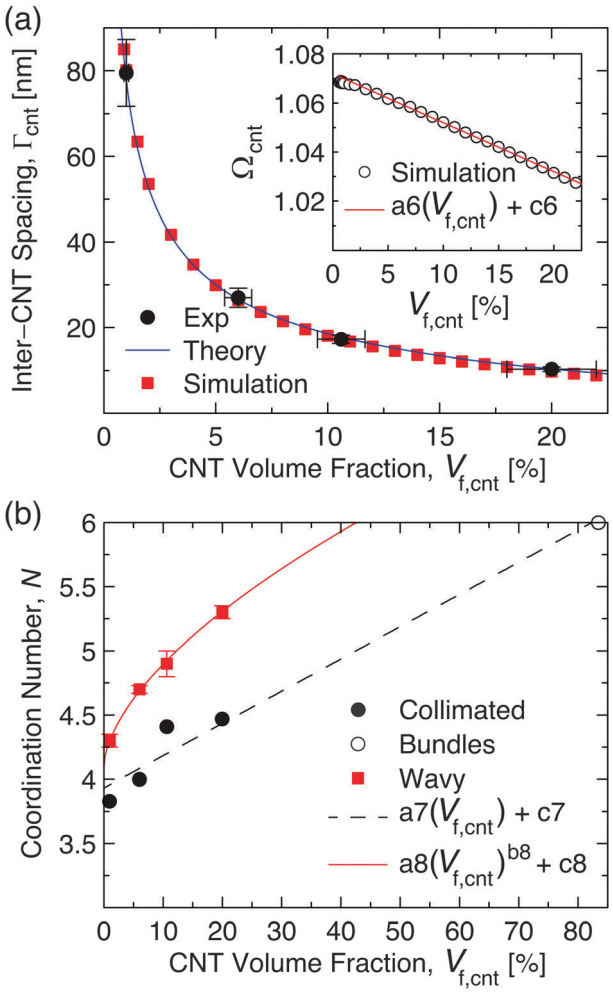

Fig. 4 Evolution of morphology of aligned carbon nanotubes (A-CNTs) as a function of their volume fraction ($V_{\mathrm{f,cnt}}$). (a) Experimentally determined inter-CNT spacing (Γ_{cnt}) as a function of V_{f},[35] previously reported theoretical scaling of Γ_{cnt} with $V_{\mathrm{f,cnt}}$ for collimated A-CNTs,[35] and the simulated scaling of Γ_{cnt} with V_{f} for wavy A-CNTs. Inset: Scaling of the waviness correction for A-CNTs (Ω_{cnt}) with $V_{\mathrm{f,cnt}}$. (b) The coordination number (N) evolution during packing resulting from the previously reported theoretical scaling for collimated A-CNTs and their bundles,[35] and the simulated scaling for wavy A-CNTs showing that integration of CNT waviness into the theoretical framework is necessary to attain a coordination number scaling that is applicable beyond $V_{\mathrm{f,cnt}} = 20\%$.

$V_{\mathrm{f,cnt}}$ ($\rightarrow -0.002V_{\mathrm{f,cnt}} + 1.072$ at a coefficient of determination $\mathbb{R}^2 = 0.9969$). See Table S2 in the ESI,† for the calculated Γ_{cnt} and Ω_{cnt} values as a function of $V_{\mathrm{f,cnt}}$ using the simulated wavy CNT arrays. Using these simulation results, N was re-evaluated for CNTs with more realistic morphologies (see Fig. 4b). As Fig. 4b illustrates, the scaling of N with $V_{\mathrm{f,cnt}}$ for wavy A-CNTs is very different from the previously reported linear scaling relation for collimated CNTs, and has the following form:

$$N(V_{\mathrm{f,cnt}}) = \begin{cases} a8(V_{\mathrm{f,cnt}})^{b8} + c8, & V_{\mathrm{f,cnt}} \lessapprox 40\% \\ 6, & V_{\mathrm{f,cnt}} \gtrapprox 40\% \end{cases} \quad (2)$$

where $a8 = 0.2$, $b8 = 0.6$, and $c8 = 4.1$ at $\mathbb{R}^2 = 0.9984$. See Table S3 in the ESI,† for the calculated values of N for the wavy A-CNT arrays. Eqn (2) indicates that at $V_{\mathrm{f,cnt}} \approx 40\%$ CNTs, hexagonal

(N = 6) packing is exhibited throughout the CNT arrays. This makes sense because spatial inhomogeneities in both Γ_{cnt} and $V_{f,cnt}$ are very significant at low ($\lesssim 10 \times \rightarrow V_{f,cnt} \sim 10\%$) densifications,[36] but becomes much less pronounced in higher densifications due to CNT–CNT confinement/proximity interactions.[42] These CNT–CNT proximity interactions, which were previously shown to have a significant influence on the CNT array behavior at $V_{f,cnt} \gtrsim 5\%$,[36] will lead the CNTs to transition from the as-grown square (N = 4) packing structure to the lower energy, and more ideal, hexagonal (N = 6) close packing structure. Further work is required to quantify the impact of the CNT proximity/confinement interactions on the evolution of the packing morphology of A-CNT arrays during densification.

In summary, a highly scalable simulation comprised of $>10^5$ nanofibers (NFs) with realistic morphologies was used to quantify the impact of NF waviness on an easily accessible measure of the morphology, the average inter-NF separation (Γ), and to study the evolution of the packing structure of an exemplary system of carbon nanotube (CNT) arrays by evaluating their effective two-dimensional coordination number. The simulation results demonstrate that oversimplifying or neglecting the NF waviness can lead to errors in Γ that may exceed 10%, and that the ideal hexagonal close packing is best suited for NF arrays with minimal waviness, whereas square close packing (N = 4) works best for NF arrays with noticeable waviness (waviness ratios >0.1). Using previously reported experimental values of the Γ and waviness ratio (w) as a function of the CNT volume fraction,[30,35] the simulation shows that N increases much faster than previously expected as the aligned CNT arrays are being densified, and that the CNT morphology can be adequately described using hexagonal close packing (in conjunction with waviness) at volume fractions $\gtrsim$20%. Since the inter-NF proximity effects can strongly influence the evolution of the packing morphology of aligned NF arrays, but their precise contribution is not currently known, additional work is required to quantify the impact of NF–NF interactions as a function of Γ. Once the NF proximity interactions can be accurately described as a function of the inter-NF separation, this simulation scheme could accurately predict the evolution of the NF morphology during packing, potentially enabling the design and fabrication of higher performing devices, such as membranes for water filtration whose permeability directly relates to the morphology,[40,43] or NF architectures with tunable mechanical behavior, where the waviness governs the stiffness.[30]

Acknowledgements

This work was supported by Airbus Group, Boeing, Embraer, Lockheed Martin, Saab AB, TohoTenax, and ANSYS through MIT's Nano-Engineered Composite aerospace STructures (NECST) Consortium and was supported (in part) by the U.S. Army Research Office under contract W911NF-07-D-0004 and W911NF-13-D-0001. I. Y. S. was supported by the Department of Defense (DoD) through the National Defense Science & Engineering Graduate Fellowship (NDSEG) Program. The authors thank Diana Lewis (MIT), John Kane (MIT) and the entire necstlab at MIT for technical support and advice. This work made use of the core facilities at the Institute for Soldier Nanotechnologies at MIT, supported in part by the U.S. Army Research Office under contract W911NF-07-D-0004, and was carried out in part through the use of MIT's Microsystems Technology Laboratories.

References

1 M. F. L. De Volder, S. H. Tawfick, R. H. Baughman and A. J. Hart, *Science*, 2013, **339**, 535–539.
2 N. P. Dasgupta, J. Sun, C. Liu, S. Brittman, S. C. Andrews, J. Lim, H. Gao, R. Yan and P. Yang, *Adv. Mater.*, 2014, **26**, 2137–2184.
3 L. Liu, W. Ma and Z. Zhang, *Small*, 2011, **7**, 1504–1520.
4 R. Agrawal, B. Peng, E. E. Gdoutos and H. D. Espinosa, *Nano Lett.*, 2008, **8**, 3668–3674.
5 R. Agrawal, B. Peng and H. D. Espinosa, *Nano Lett.*, 2009, **9**, 4177–4183.
6 H. D. Espinosa, R. A. Bernal and M. Minary-Jolandan, *Adv. Mater.*, 2012, **24**, 4656–4675.
7 A. A. Balandin, *Nat. Mater.*, 2011, **10**, 569–581.
8 A. M. Marconnet, M. A. Panzer and K. E. Goodson, *Rev. Mod. Phys.*, 2013, **85**, 1295–1326.
9 K. H. Baloch, N. Voskanian, M. Bronsgeest and J. Cumings, *Nat. Nanotechnol.*, 2012, **7**, 316–319.
10 Y. Lisunova, I. Levkivskyi and P. Paruch, *Nano Lett.*, 2013, **13**, 4527–4531.
11 D. Papkov, Y. Zou, M. N. Andalib, A. Goponenko, S. Z. D. Cheng and Y. A. Dzenis, *ACS Nano*, 2013, **7**, 3324–3331.
12 A. M. Marconnet, N. Yamamoto, M. A. Panzer, B. L. Wardle and K. E. Goodson, *ACS Nano*, 2011, **5**, 4818–4825.
13 N. J. Ginga, W. Chen and S. K. Sitaraman, *Carbon*, 2014, **66**, 57–66.
14 F. T. Fisher, R. D. Bradshaw and L. C. Brinson, *Appl. Phys. Lett.*, 2002, **80**, 4647–4649.
15 F. Fisher, R. Bradshaw and L. Brinson, *Compos. Sci. Technol.*, 2003, **63**, 1689–1703.
16 E. Shady and Y. Gowayed, *Compos. Sci. Technol.*, 2010, **70**, 1476–1481.
17 A. Y. Matveeva, S. V. Pyrlin, M. M. Ramos, H. J. Böhm and F. W. van Hattum, *Comput. Mater. Sci.*, 2014, **87**, 1–11.
18 S. Paunikar and S. Kumar, *Comput. Mater. Sci.*, 2014, **95**, 21–28.
19 U. Vainio, T. I. W. Schnoor, S. Koyiloth Vayalil, K. Schulte, M. Müller and E. T. Lilleodden, *J. Phys. Chem. C*, 2014, **118**, 9507–9513.
20 D. N. Futaba, K. Hata, T. Yamada, T. Hiraoka, Y. Hayamizu, Y. Kakudate, O. Tanaike, H. Hatori, M. Yumura and S. Iijima, *Nat. Mater.*, 2006, **5**, 987–994.
21 B. L. Wardle, D. S. Saito, E. J. García, A. J. Hart, R. Guzmán de Villoria and E. A. Verploegen, *Adv. Mater.*, 2008, **20**, 2707–2714.
22 Q. Jiang, S. S. Tallury, Y. Qiu and M. A. Pasquinelli, *Carbon*, 2014, **67**, 440–448.

23 K. Chae and L. Huang, *J. Phys. Chem. C*, 2015, **119**, 6806–6812.
24 M. Rahimi, J. K. Singh, D. J. Babu, J. J. Schneider and F. Müller-Plathe, *J. Phys. Chem. C*, 2013, **117**, 13492–13501.
25 M. Rahimi, D. J. Babu, J. K. Singh, Y.-B. Yang, J. J. Schneider and F. Müller-Plathe, *J. Chem. Phys.*, 2015, **143**, 124701.
26 M. Rahimi, J. K. Singh and F. Müller-Plathe, *J. Phys. Chem. C*, 2015, **119**, 15232–15239.
27 H. Cebeci, R. Guzmán de Villoria, A. J. Hart and B. L. Wardle, *Compos. Sci. Technol.*, 2009, **69**, 2649–2656.
28 D. Handlin, I. Y. Stein, R. Guzman de Villoria, H. Cebeci, E. M. Parsons, S. Socrate, S. Scotti and B. L. Wardle, *J. Appl. Phys.*, 2013, **114**, 224310.
29 J. Lee, I. Y. Stein, M. E. Devoe, D. J. Lewis, N. Lachman, S. S. Kessler, S. T. Buschhorn and B. L. Wardle, *Appl. Phys. Lett.*, 2015, **106**, 053110.
30 I. Y. Stein, D. J. Lewis and B. L. Wardle, *Nanoscale*, 2015, **7**, 19426–19431.
31 J.-Q. Huang, Q. Zhang, G.-H. Xu, W.-Z. Qian and F. Wei, *Nanotechnology*, 2008, **19**, 435602.
32 Y. Zhang, G. Zou, S. K. Doorn, H. Htoon, L. Stan, M. E. Hawley, C. J. Sheehan, Y. Zhu and Q. Jia, *ACS Nano*, 2009, **3**, 2157–2162.
33 S. Pathak, J. R. Raney and C. Daraio, *Carbon*, 2013, **63**, 303–316.
34 M. Bedewy and A. J. Hart, *Nanoscale*, 2013, **5**, 2928–2937.
35 I. Y. Stein and B. L. Wardle, *Phys. Chem. Chem. Phys.*, 2013, **15**, 4033–4040.
36 I. Y. Stein, N. Lachman, M. E. Devoe and B. L. Wardle, *ACS Nano*, 2014, **8**, 4591–4599.
37 S. Cranford, H. Yao, C. Ortiz and M. J. Buehler, *J. Mech. Phys. Solids*, 2010, **58**, 409–427.
38 Y. Won, Y. Gao, M. A. Panzer, R. Xiang, S. Maruyama, T. W. Kenny, W. Cai and K. E. Goodson, *Proc. Natl. Acad. Sci. U. S. A.*, 2013, **110**, 20426–20430.
39 M. R. Maschmann, *Carbon*, 2015, **86**, 26–37.
40 B. Lee, Y. Baek, M. Lee, D. H. Jeong, H. H. Lee, J. Yoon and Y. H. Kim, *Nat. Commun.*, 2015, **6**, 7109.
41 B. Natarajan, N. Lachman, T. Lam, D. Jacobs, C. Long, M. Zhao, B. L. Wardle, R. Sharma and J. A. Liddle, *ACS Nano*, 2015, **9**, 6050–6058.
42 H. Cebeci, I. Y. Stein and B. L. Wardle, *Appl. Phys. Lett.*, 2014, **104**, 023117.
43 S. Wang, D. Haldane, R. Liang, J. Smithyman, C. Zhang and B. Wang, *Nanotechnology*, 2013, **24**, 015704.